



# Predictive design of $\text{KSnI}_3$ -based perovskite solar cells using SCAPS and machine learning model

Rahul Kundara<sup>\*</sup>, Sarita Baghel

*Department of Applied Physics, Delhi Technological University, Delhi, India*



## ARTICLE INFO

### Keywords:

$\text{KSnI}_3$ -based PSC

SCAPS-1D

Machine learning and HTLs

## ABSTRACT

The commercial application of lead (Pb)-based Perovskite Solar Cells (PSCs) are restrained due to its toxicity. In this work, we have investigated potassium tin iodide ( $\text{KSnI}_3$ ) which is a potential candidate for non-lead PSC. The SCAPS-1D simulation is employed to examine the effect of several Hole Transport Layers (HTLs) as follow: Spiro-OMeTAD, CuI, CuSCN,  $\text{Cu}_2\text{O}$ , PEDOT: PSS, CdTe,  $\text{MASnBr}_3$ , CFTS on the performance of  $\text{KSnI}_3$ -based PSCs. The impact of layer thickness, doping density ( $N_A$ ) and defect density ( $N_t$ ) has been analyzed. We have a trained Machine learning model to predict the performance matrices of PSCs. We have obtained a maximum efficiency of 23.08 % at the thickness of the  $\text{KSnI}_3$  absorber layer of 550 nm and  $N_t$  of  $10^{13} \text{ cm}^{-3}$ . The ML model predicts the performance matrices of examined PSC with accuracy of ~ 89 %. Hence, the FTO/WS<sub>2</sub>/ $\text{KSnI}_3$ /PEDOT: PSS/Au configuration is most suitable to manufacture highly efficient PV devices.

## 1. Introduction

Utilizing solar cells for solar energy harvesting presents a commendable approach mitigating concerns about global warming. The photovoltaic effect converts incident sunlight into electrical energy. In 2009, Perovskite solar cell (PSC) was reported with an efficiency of 3.8 % and has achieved maximum power conversion efficiency (PCE) of greater than 26 % till now [1]. It became popular among the scientific community due to its promising attributes such as tunable bandgap ( $E_g$ ), high absorption coefficient, high carrier mobility, low manufacturing cost and high PCE or efficiency [2,3]. Perovskite material has an ABX<sub>3</sub> structure (where A is an organic or inorganic cation, B is an inorganic metal cation and X is halogen anion) [4]. Despite the high performance of lead (Pb) based PSC, its instability due to rapid oxidation of Pb cation and toxic nature restricted its commercialization [5]. There is a need for alternative perovskite materials that are both less toxic and environmentally friendly while also having the potential to deliver exhibit good photovoltaic (PV) outcomes [6]. Hence there have been various investigations to replace hazardous Pb ions with other alternatives such as Sn [7], Ge [8], Bi [9], Sb [10] and Ag [11]. The tin (Sn) is a suitable choice due to comparable ionic radii and the phenomenal semiconducting properties of APbX<sub>3</sub>. The study comprises investigation of  $\text{KSnI}_3$  as a perovskite material which is used as an absorber in a PSC. In past reported investigations there is very limited study on  $\text{KSnI}_3$  PSC.

Grishma et al. (2023) have reported efficiency of 9.77 % [12]. So there needs to be proper optimization to enhance the efficiency of PSC. Whereas, in this work we have obtained a maximum PCE of 23.08 %. The SCAPS enabled machine learning model is used to optimize and predict the best efficiency [13]. It has been exhibited that ML is helpful in forecasting the design and performance of PSCs [14]. Firstly, we have simulated  $\text{KSnI}_3$ -based PSC with several HTLs (Spiro-OMeTAD, CuI, CuSCN,  $\text{Cu}_2\text{O}$ , PEDOT: PSS, CdTe,  $\text{MASnBr}_3$  and CFTS) and  $\text{KSnI}_3$  is employed as a perovskite absorber layer. Secondly, we have optimized the effect of distinct performance parameters of PSCs such as absorber layer thickness, defect density ( $N_t$ ) and doping density ( $N_A$ ). Ultimately, we trained an ML model to predict the performance parameters of the PSCs with an accuracy of approximately 89 %. The present method serves as a sturdy foundation for subsequent research and investigations driven by artificial intelligence (AI). The efficient PSCs can be designed with application of ML modelling and SCAPS-1D assisted by previous studies.

## 2. Device architecture and methods

The PSC consists of  $\text{KSnI}_3$  absorber material with layer architecture: FTO/ETL/Perovskite layer/HTL/Back-contact depicted in Fig. 1. All the input data used in SCAPS simulation obtained from experimental and theoretical work enclosed is in Table 1 for FTO/TiO<sub>2</sub>/ $\text{KSnI}_3$ /Spiro-

\* Corresponding author.

E-mail address: [rahul\\_2k20phdap10@dtu.ac.in](mailto:rahul_2k20phdap10@dtu.ac.in) (R. Kundara).

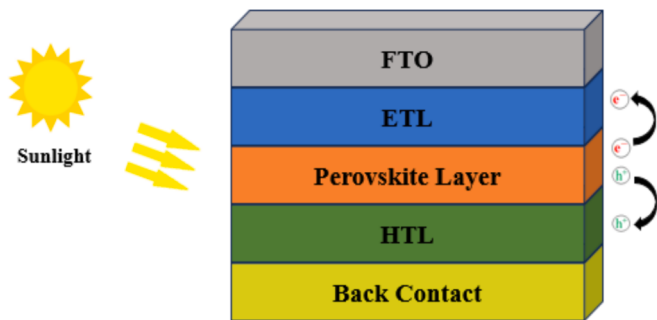


Fig. 1. Architecture of simulated PSCs.

**Table 1**  
Input parameters of simulated PSC.

Parameter	FTO [15,16]	WS <sub>2</sub> [17]	KSnI <sub>3</sub> [12]	Spiro-OMeTAD [18,19]
Thickness (nm)	400	100*	300	50
Eg (eV)	3.5	1.8	1.84	3.0
$\chi$ (eV)	4.0	3.95	3.44	2.45
$\epsilon$	9.0	13.6	10.4	3.0
N <sub>C</sub> (cm <sup>-3</sup> )	$2.02 \times 10^{18}$	$1 \times 10^{18}$	$2.2 \times 10^{18}$	$1 \times 10^{19}$
N <sub>V</sub> (cm <sup>-3</sup> )	$1.8 \times 10^{19}$	$2.4 \times 10^{19}$	$1.8 \times 10^{19}$	$1 \times 10^{19}$
$\mu_n$ (cm <sup>2</sup> /Vs)	20	$10^{19}$	21.28	$1 \times 10^{-4}$
$\mu_p$ (cm <sup>2</sup> /Vs)	10	100	19.46	$1 \times 10^{-4}$
N <sub>D</sub> (cm <sup>-3</sup> )	$2 \times 10^{19}$	$1 \times 10^{18}$	$1 \times 10^{15}$	0
N <sub>A</sub> (cm <sup>-3</sup> )	0	0	$1 \times 10^{15}$	$2 \times 10^{18}$
N <sub>t</sub> (cm <sup>-3</sup> )	$1 \times 10^{15}$	$1 \times 10^{13*}$	$1 \times 10^{13}$	$1 \times 10^{14}$

OMeTAD/Au-Metal and HTLs in Table 2.

### 2.1. SCAPS-1D

The data of different parameters are chosen from previous studies. The SCAPS-1D (version 3.3.10) has been employed for simulation. This software can be used for simulations at different input physical conditions. This tool calculation is dependent on Poisson's and continuity equations. It can calculate Quantum efficiency (QE), J-V curve and carrier lifetime for both electrons (e<sup>-</sup>s) and holes (h<sup>+</sup>s).

$$\frac{\partial^2 \psi}{\partial x^2} + \frac{q}{\epsilon} [p(x) - n(x) + N_D - N_A + \rho_p - \rho_n] = 0 \quad (1)$$

$$\frac{1}{q} \frac{dJ_p}{dx} = G_{op}(x) - R(x) \quad (2)$$

$$\frac{1}{q} \frac{dJ_n}{dx} = -G_{op}(x) + R(x) \quad (3)$$

The simulations were run at 300 K using a “air mass 1.5 global” spectrum and a light power of 1000 W/m<sup>2</sup>. The work is dependent on change in thickness, N<sub>b</sub>, and N<sub>A</sub> at which simulation of the proposed PSC has been done. The outcome of the device has been reflected by the I-V characteristics which represent the following PV parameters: J<sub>SC</sub>, FF, V<sub>OC</sub>, and PCE. The simulation procedure is depicted in Fig. 2.

### 2.2. Machine learning

Python was chosen as the programming language for implementing machine learning (ML) due to its widespread use in AI applications [27–29]. To work with the dataset, Numpy and Pandas libraries were utilized. The dataset pertains to solar cell features and was thoroughly cleaned and preprocessed to make it compatible with ML algorithms. Initially, a simple Random Forest algorithm from Scikit-Learn (Sklearn) was employed to determine the significance of each feature for the final model. As a result of this phase, eleven features were selected for further analysis. For feature extraction related to composition of perovskites, Pymatgen and Matminer packages were utilized. The data was then split

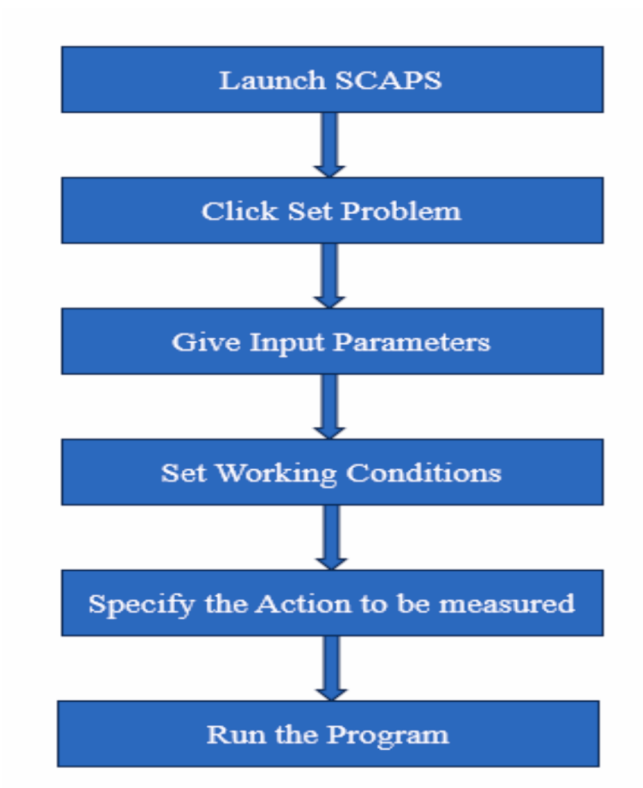


Fig. 2. SCAPS-1D simulation procedure.

**Table 2**  
Input parameters of distinct HTLs.

Parameter	CuI [18,19]	CuSCN [19,20]	Cu <sub>2</sub> O [15,19,21]	PEDOT: PSS [19,22,23]	CdTe [19,24]	MASnBr <sub>3</sub> [6,19,25]	CFTS [19,26]
Thickness (nm)	50	50	50	50	50	50	50
Eg (eV)	3.1	3.4	2.17	2.2	1.5	2.15	1.3
$\chi$ (eV)	2.1	1.9	3.2	2.9	3.9	3.39	3.3
$\epsilon$	6.5	10	7.11	3.0	9.4	8.2	9.0
N <sub>C</sub> (cm <sup>-3</sup> )	$2.8 \times 10^{19}$	$2.2 \times 10^{19}$	$2.02 \times 10^{17}$	$2.2 \times 10^{15}$	$8.0 \times 10^{17}$	$1 \times 10^{18}$	$2.2 \times 10^{18}$
N <sub>V</sub> (cm <sup>-3</sup> )	$1 \times 10^{19}$	$1.8 \times 10^{18}$	$1.1 \times 10^{19}$	$1.8 \times 10^{18}$	$1.8 \times 10^{19}$	$1 \times 10^{18}$	$1.8 \times 10^{19}$
$\mu_n$ (cm <sup>2</sup> /Vs)	100	$1 \times 10^{-4}$	200	$1 \times 10^{-2}$	$3.2 \times 10^2$	1.6	21.98
$\mu_p$ (cm <sup>2</sup> /Vs)	80	$1 \times 10^{-2}$	80	$2 \times 10^{-4}$	40	1.6	21.98
N <sub>D</sub> (cm <sup>-3</sup> )	0	0	0	0	0	0	0
N <sub>A</sub> (cm <sup>-3</sup> )	$1 \times 10^{18}$	$1 \times 10^{16}$	$1 \times 10^{18}$	$1 \times 10^{19}$	$2 \times 10^{14}$	$1 \times 10^{18}$	$1 \times 10^{18}$
N <sub>t</sub> (cm <sup>-3</sup> )	$1 \times 10^{14}$	$1 \times 10^{14*}$	$1 \times 10^{14}$	$1 \times 10^{14}$	$1 \times 10^{14*}$	$1 \times 10^{14*}$	$1 \times 10^{14*}$

into training and testing sets for model training. To find the best hyperparameters, two distinct approaches were taken. First a parameter grid (a Python dictionary) inclusive various values for each parameter was prepared. The RandomizedSearchCV and GridSearchCV tools from Scikit-Learn were employed to assess the optimal combination of hyperparameters from this grid. The RandomizedSearchCV randomly selected combinations from the grid and evaluated their performance using cross-validation, while the GridSearchCV evaluated every possible combination of the provided parameters. To ensure the model's performance and consistency, five-fold cross-validation was performed on the final model. Subsequently, a separate test set was used to assess the model's accuracy and overall performance. Random Forest's ability to aggregate the results of individual decision trees helped mitigate overfitting issues and improved the model's predictive performance [30]. Overfitting occurs when a model becomes too tailored to the training data, resulting in high variance and poor predictive performance on the test set. To mitigate overfitting, various techniques can be applied, such as comparing the prediction results between the training and test sets. Several approaches can be used, including increasing the number of decision trees and reducing their maximum depth. The prediction's coefficient of determination acted as the evaluation metric. According to the Sklearn, this metric exhibited as is defined as:

$R^2 = \left(1 - \frac{u}{v}\right)$  (4). u represent the residual sum of squares ( $(y_{\text{pred}} - y_{\text{true}})^2$ ). Meanwhile, v stands for the total sum of squares =  $((y_{\text{pred}} - \text{mean}(y_{\text{true}}))^2$ . It's worth noting that a constant model that solely predicts the anticipated y, irrespective of input, could obtain a score of  $R^2$  equal to 0.0. The significance of a node j within a single decision tree, the calculation involved as follows [30]:

$$ni_j = w_j C_j - w_{\text{left}(j)} C_{\text{left}(j)} - w_{\text{right}(j)} C_{\text{right}(j)} \quad (5)$$

where  $w_j$  denotes the weighted number of samples in node j as a fraction of the total weighted number of samples.  $C_j$  represents the impurity in node j and left (j) and right (j) corresponds to the child nodes associated with it. The following calculation is used to determine feature's importance [30]:

$$fi_i = \frac{\sum_{j: \text{node } j \text{ splits on feature } i} ni_j}{\sum_{j: \text{all nodes}} ni_j} \quad (6)$$

Ultimately, the feature values were calculated as the mean of every particular decision tree.

### 3. Results and discussion

#### 3.1. HTL

The HTL exhibits an important role in optimization of PSC performance via two ways such as it transports the light generated holes towards the back contact and HTL hampers the interaction between absorber layer and back contact. Despite the comprehensive application of Spiro-OMeTAD into PSC to increase PCE, low hole mobility ( $\mu_p$ ), and environment instability confined its commercial application. Consequently, various kinds of HTLs like CuI, CuSCN, Cu<sub>2</sub>O, PEDOT: PSS, CdTe, MASnBr<sub>3</sub> and CFTS have been analyzed shown in Table 2. To begin the simulation, a PSC architecture of FTO/TiO<sub>2</sub>/KSnI<sub>3</sub>/Spiro-OMeTAD/Au was simulated to validate with previously reported results [8]. WS<sub>2</sub> opted as ETL due to its high electron mobility ( $\mu_n$ ), wide range of  $E_g$ , and high conductivity of  $10^{-3} \Omega^{-1} \text{ cm}^{-1}$  [31]. The validation of the simulated result shown below in Table 3. The highest occupied molecular orbital (HOMO) of HTL should be appropriately aligned with that of the perovskite layer. The proper optimization is required to select appropriate ETL and HTL to maximize the performance of the PSC. The energy bandgap diagram of ETL, absorber layer and various HTLs illustrated below in Fig. 3. The J-V and QE plots of PSC with various HTLs are shown below in Fig. 4. The plotted curve from simulations is

**Table 3**

Comparison with previously reported results.

Cell structure	V <sub>OC</sub> (V)	J <sub>SC</sub> (mA/cm <sup>2</sup> )	FF (%)	PCE (%)
FTO/TiO <sub>2</sub> /KSnI <sub>3</sub> /Spiro-OMeTAD/W	1.70	15.85	36.13	9.77 [8]
FTO/C <sub>60</sub> /KSnI <sub>3</sub> /PTAA/C	0.76	17.44	80.80	10.83 [32]
FTO/TiO <sub>2</sub> /KSnI <sub>3</sub> /Spiro-OMeTAD/Au	1.48	13.20	79.07	15.55 [This work]

well-fitted with the previously reported outcomes, which validates numerical simulations.

To examine the impact of the several HTLs like Spiro-OMeTAD, CuI, CuSCN, Cu<sub>2</sub>O, PEDOT: PSS, CdTe, MASnBr<sub>3</sub> and CFTS on the PV parameters of PSC. The thickness of HTLs was 50 nm throughout the simulation. The simulated results are demonstrated in Fig. 4. The PV parameters with several HTLs are presented below in Table 4.

The Spiro-OMeTAD and PEDOT: PSS both are organic materials. The  $E_g$  for Spiro-OMeTAD is 3 eV and for PEDOT: PSS is 2.2 eV depicted in table 1 and 2. The PEDOT: PSS has excellent properties such as high electrical conductivity, mechanical flexibility and suitable for thin film formation [33]. The simulation results demonstrated that KSnI<sub>3</sub>-based PSC exhibited maximum PCE of 21.08 % (with V<sub>OC</sub> of 1.59 V, J<sub>SC</sub> of 15.08 mA/cm<sup>2</sup> and FF of 87.43 %) for WS<sub>2</sub> as ETL and PEDOT: PSS employed as HTL. The HOMO level of Spiro-OMeTAD and PEDOT: PSS has good band alignment with KSnI<sub>3</sub> therefore with PEDOT: PSS it has achieved maximum PCE but not for Spiro-OMeTAD. This can be attributed to lower hole mobility ( $\mu_p$ ) than PEDOT: PSS [34,35]. Hence, PEDOT: PSS is an appropriate HTL for achieving high PCE. Furthermore, the PEDOT: PSS exhibits good stability in air over Spiro-OMeTAD so that it has wide application in PSCs. Zuo et al. (2017) doped PEDOT: PSS with polymer electrolyte PSS-Na which results in high work function and good band alignment of modified PEDOT: PSS with the absorber layer. Hence, enhanced PCE has been obtained from 12.35 % to 15.56 % [36]. The small amount of 2,3,5,6-tetrafluoro-7,7,8,8-tetracyanoquinodimethane (F4-TCNQ) added to PEDOT: PSS could improve the electrical conductivity and better band matching with the absorber layer. Therefore, the PCE enhanced from 13.30 % to 17.22 % [37,38].

#### 3.2. Optimization of HTL

##### 3.2.1. Impact of thickness

In the preceding section, Table 4 highlighted that PEDOT: PSS emerges as the most promising HTL for KSnI<sub>3</sub>-based PSC. As the attributes of HTL, such as thickness, doping density (N<sub>A</sub>), and defect density (N<sub>t</sub>), exert a substantial influence on PSC performance and these parameters must be optimized. Notably, HTL thickness exhibits a vital role in facilitating efficacious carrier transport and controlling the recombination rate [39]. Consequently, the thickness of an HTL is optimized to get high PCE. Fig. 5a, b demonstrates the impact of PEDOT: PSS thickness on the J<sub>SC</sub> and V<sub>OC</sub> of PSCs. The findings reveal that increasing PEDOT: PSS thickness up to 250 nm enhances both J<sub>SC</sub> and V<sub>OC</sub>, beyond which they become constant. According to experimental surveys, thicker HTLs yields smoother film surfaces, reducing interfacial recombination and thus enhancing V<sub>OC</sub>. The suitable HTL thickness is required to avoid series resistance (R<sub>S</sub>) for thicker layers [40,41]. Firstly, a thinner HTL might not accumulate a sufficient number of holes. Secondly, the region among the absorber layer and a thin HTL might not be as potent as in thicker layers, leading to inadequate driving force for carrier partition. The study also indicates that when HTL thickness exceeds 250 nm both V<sub>OC</sub> and J<sub>SC</sub> tend to be constant. This is primarily due to carrier travel distance to reach the interface. Consequently, traps promote non-radiative Shockley–Read–Hall (SRH) recombination and enhanced trap-assisted recombination rate [42]. The influence of thickness on PV parameters is depicted in Fig. 5. The initial fall in the

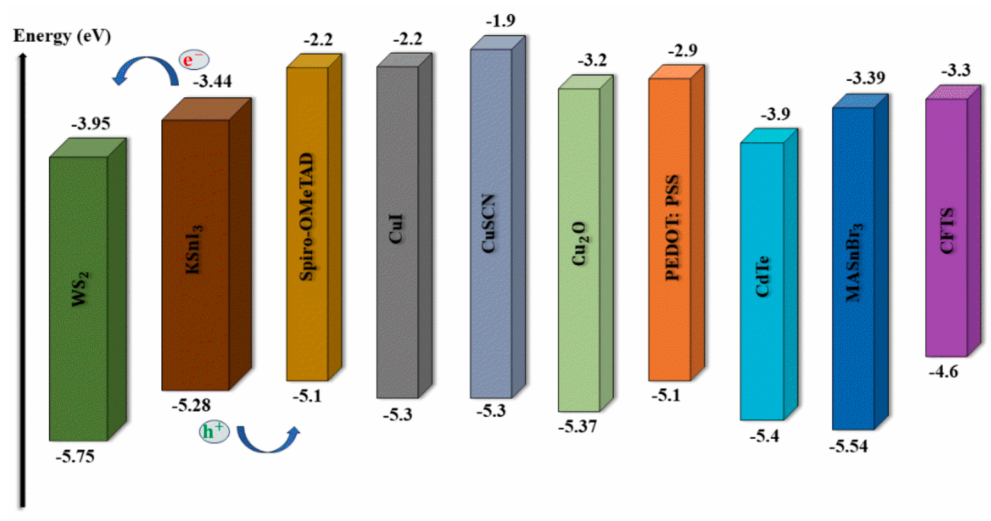


Fig. 3. Energy band diagram of various HTLs.

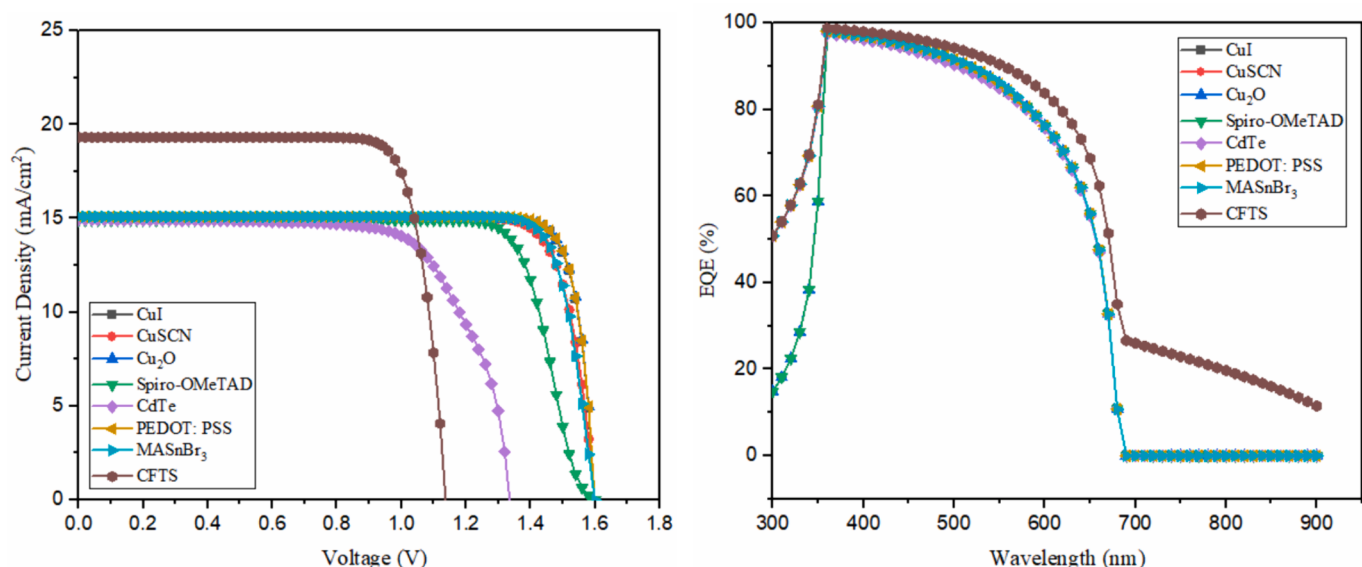


Fig. 4. (a) J-V and (b) QE plots of simulated PSCs with various HTLs.

**Table 4**  
The PV parameters of KSnI<sub>3</sub>-based PSC with distinct HTLs.

Cell structure	V <sub>OC</sub> (V)	J <sub>SC</sub> (mA/cm <sup>2</sup> )	FF (%)	PCE (%)
FTO/WS <sub>2</sub> /KSnI <sub>3</sub> /CuI/Au	1.59	15.01	87.40	20.98
FTO/WS <sub>2</sub> /KSnI <sub>3</sub> /CuSCN/Au	1.59	15.01	84.48	20.27
FTO/WS <sub>2</sub> /KSnI <sub>3</sub> /Cu <sub>2</sub> O/Au	1.59	14.96	87.63	20.96
FTO/WS <sub>2</sub> /KSnI <sub>3</sub> /Spiro-OMeTAD/Au	1.59	14.89	79.18	18.85
FTO/WS <sub>2</sub> /KSnI <sub>3</sub> /PEDOT: PSS/Au	1.59	15.08	87.43	21.08
FTO/WS <sub>2</sub> /KSnI <sub>3</sub> /CdTe/Au	1.33	14.93	71.06	14.18
FTO/WS <sub>2</sub> /KSnI <sub>3</sub> /MASnBr <sub>3</sub> /Au	1.59	15.09	85.14	20.56
FTO/WS <sub>2</sub> /KSnI <sub>3</sub> /CFTS/Au	1.13	19.32	81.26	17.85

curve is a result of an increase in R<sub>S</sub>. The optimized thickness of HTL is 250 nm, yielding a PCE of 21.30 % demonstrated in Fig. 5d.

### 3.2.2. Impact of N<sub>A</sub>

The findings from previous studies have shown the significant impact of doping density (N<sub>A</sub>) in the HTL vastly affects the PV parameters of

PSCs, including conductivity, recombination rate and V<sub>OC</sub> [6]. Hence, the solar cell parameters were simulated in the range of N<sub>A</sub> values from 10<sup>14</sup> to 10<sup>22</sup> cm<sup>-3</sup> at a thickness of 250 nm of HTL. As depicted in Fig. 6a, an enhancement in N<sub>A</sub> leads to an increase in V<sub>OC</sub>. In layered semiconductor architectures, the alignment of the fermi level at the same value results in an equilibrium state, causing band bending and built-in voltage (V<sub>bi</sub>) [43]. This internal electric field drifts segregated photo-generated e's and h<sup>+</sup>s towards the n and p regions respectively, where they gather. Under illumination and open-circuit conditions, the excited carriers induce the separation of quasi-Fermi-levels (EFn and EFp) for e's and h<sup>+</sup>s, respectively, within the photoactive semiconductor material. This effectively nullifies V<sub>bi</sub>, and forms a photo-voltage referred to as V<sub>OC</sub> [44].

Raising the dopant concentration leads to reduction in the recombination rate, owing to an enhanced internal electric field and accelerated carrier segregation. Simultaneously, there's a slight decrease in J<sub>SC</sub> within the N<sub>A</sub> range of 10<sup>14</sup> to 10<sup>18</sup> cm<sup>-3</sup>. Notably, a pronounced fall in the J<sub>SC</sub> is observed at 10<sup>19</sup> cm<sup>-3</sup> due to generation of numerous deep Coulomb traps that reduce the μ<sub>p</sub> [45]. The Fig. 6a shows that the maximum PCE of 21.32 % is obtained at N<sub>A</sub> of 10<sup>20</sup> cm<sup>-3</sup>.

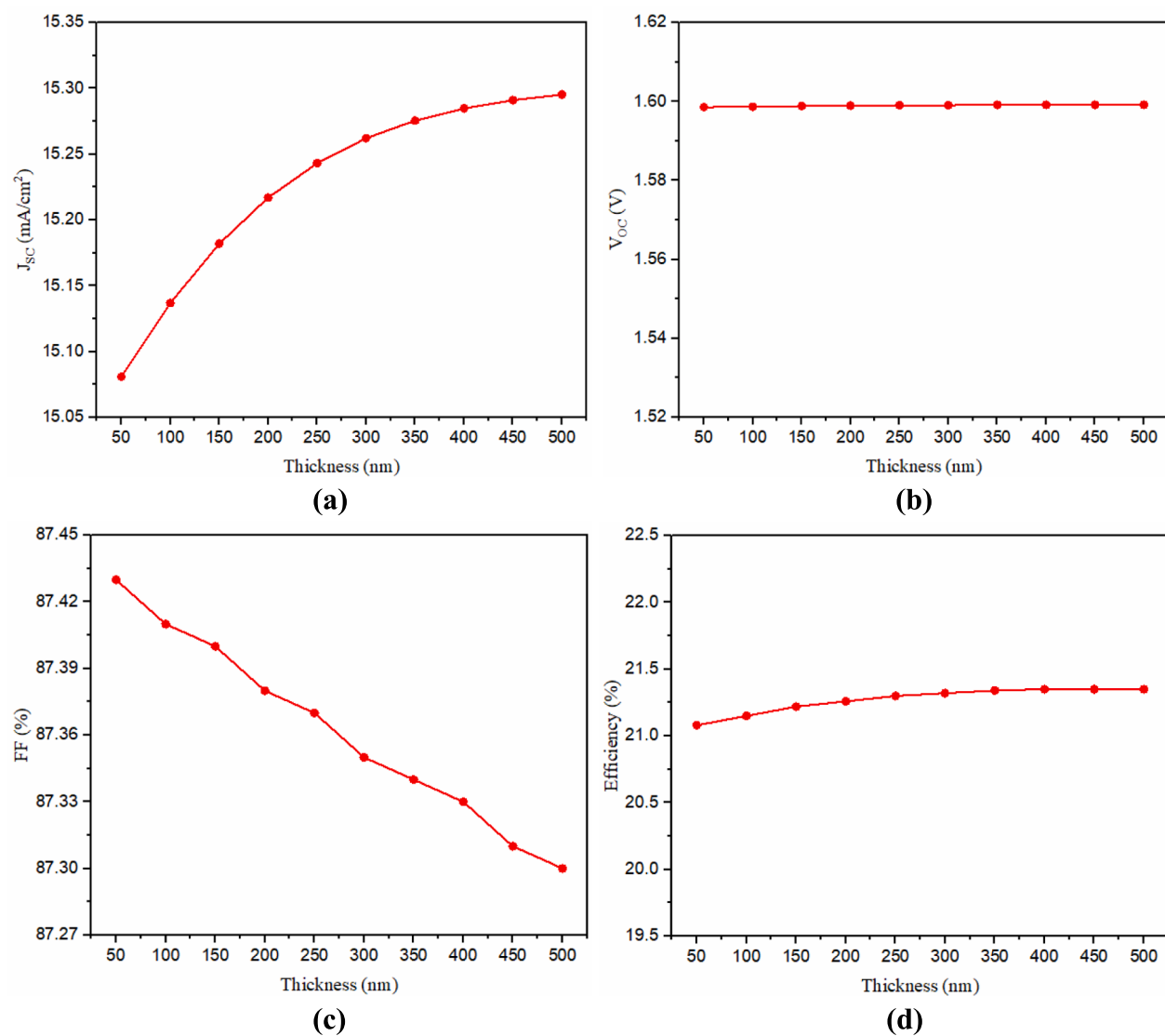


Fig. 5. Impact of the thickness of PEDOT: PSS layer on PV parameters of PSC.

### 3.2.3. Impact of $N_t$

In addition to the  $N_A$ , HTL defect density ( $N_t$ ) affects the performance of PSCs. The impact on the PSC characteristics demonstrated in Fig. 7. The  $N_t$  of  $10^{17}$  to  $10^{22}$  cm<sup>-3</sup>, Fig. 7a, b, c and d reveal no significant changes in PV parameters. However, a pronounced decline in  $V_{OC}$ ,  $J_{SC}$  and PCE surface for change in  $N_t$  from  $10^{14}$  cm<sup>-3</sup> to  $10^{17}$  cm<sup>-3</sup>. This precipitous shift is primarily attributed to the rapid emergence of numerous recombination sites in the HTL and at interfaces [46]. A high value of  $N_t$  in HTL, arising from diverse sources like undesirable foreign atoms, and native defects, give rise to shallow or deep traps. These traps adversely impact cell performance. Fig. 7d shows that an increase in interface defects leads to reduced efficiency. Beyond a certain  $N_t$ , it becomes constant. These interface defects, primarily stemming from the lattice mismatch between absorber layer (AL) and HTL, yield deep traps at the interface. These traps function as SRH recombination centers. Consequently, PCE experiences a decline, reaching about 20.97 % at  $N_t = 10^{22}$  cm<sup>-3</sup>. In the beginning FF decline is attributed to the abundance of recombination centers and  $R_S$  resulting from a significant number of traps (Fig. 7c). Despite the superior outcomes at lower  $N_t$ , simulation results diverge from experimental findings. Hence, a value of  $1 \times 10^{14}$  cm<sup>-3</sup> was selected.

### 3.3. Optimization of $KSnI_3$ layer

The above outcomes have shown that PEDOT: PSS is the most suitable HTL for  $KSnI_3$ -based PSC. The maximum PCE of beyond 21 % has been obtained at 250 nm of thickness of HTL,  $N_A$  of  $10^{20}$  cm<sup>-3</sup> and at  $N_t$  of  $1 \times 10^{14}$  cm<sup>-3</sup>. Therefore, we have opted for this optimized value of thickness,  $N_A$  and  $N_t$  for the further simulation study to optimize the performance of  $KSnI_3$ -based PSC.

#### 3.3.1. Impact of thickness

The characteristics parameters like  $J_{SC}$ ,  $V_{OC}$ , FF and PCE of PSCs are significantly influenced by the thickness of the perovskite absorber layer. In our investigation, we explored the impact of thickness of the absorber layer on the performance of the architecture: FTO/WS<sub>2</sub>(100 nm)/ $KSnI_3$ /PEDOT: PSS (250 nm)/Au. The thickness of the  $KSnI_3$  layer has exhibited a straight relation with the evaluation of the outcomes of PSC through its effect on the charge carrier's diffusion length. It is known to us that as the thickness of the layer decreases, the absorption rate also lowers. This results in a decrement in photocurrent and therefore PCE of the PSC also reduces from 200 to 1000 nm. The change in PCE is depicted below in Fig. 8a. However, with the thickness increasing up to 550 nm, PCE gradually rises. This phenomenon can be attributed to the generation of large amounts of charge carriers by

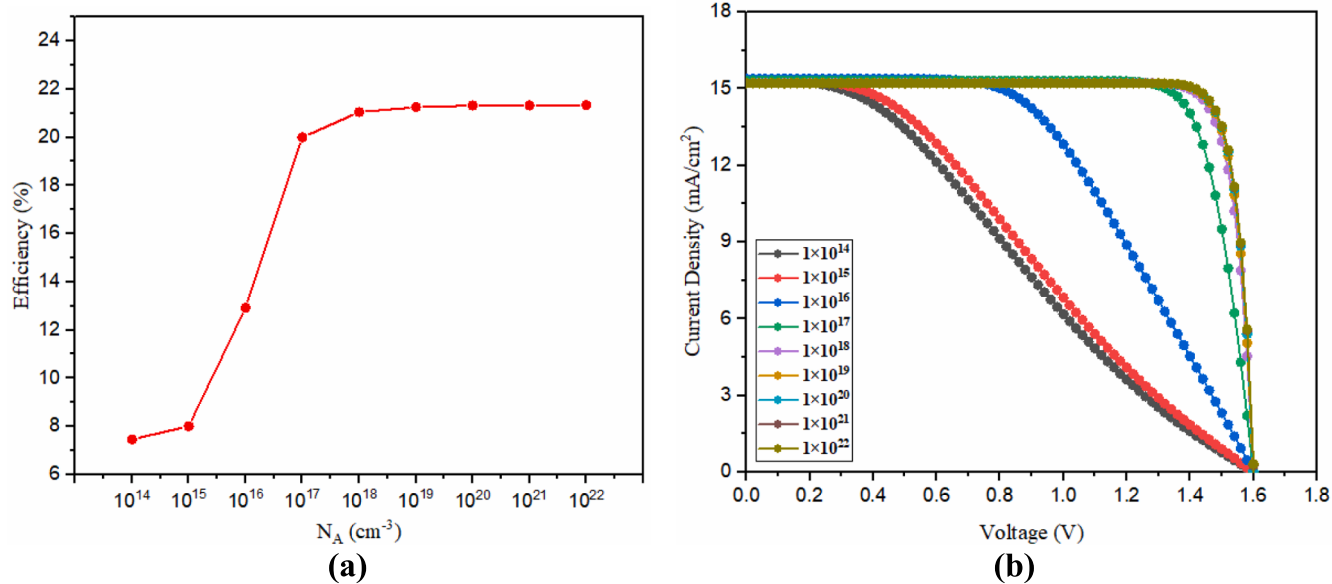


Fig. 6. (a) Efficiency versus  $N_A$  of the PEDOT: PSS. (b) J-V curves of HTL depending on its  $N_A$ .

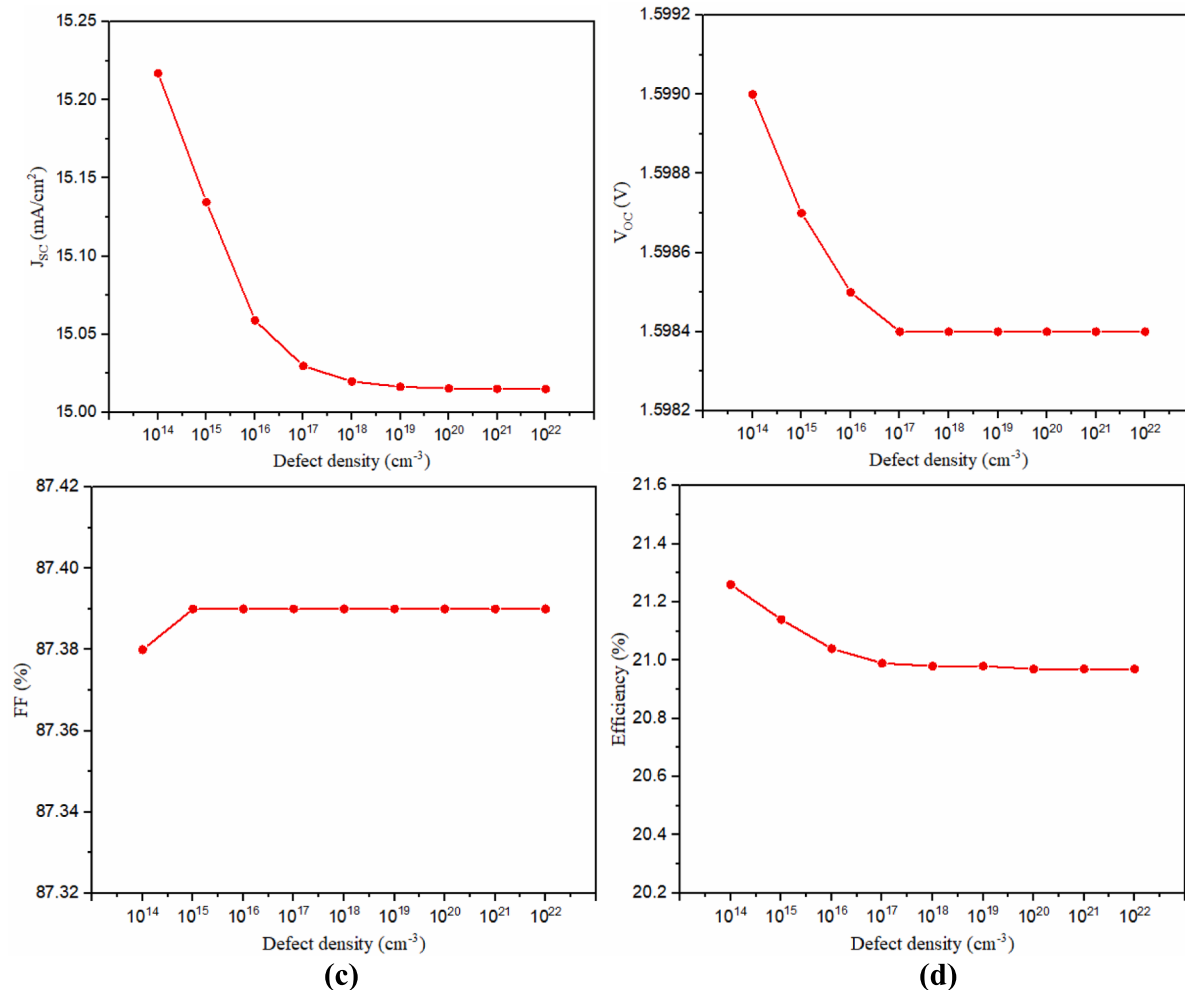
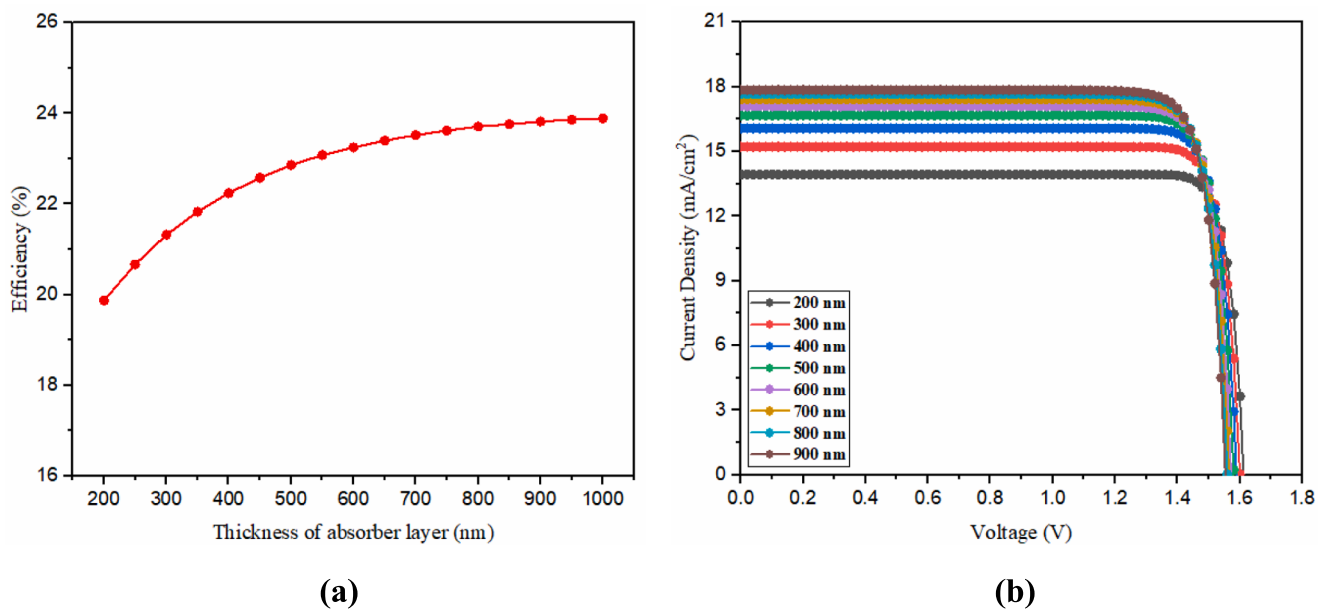


Fig. 7. Impact of  $N_t$  of the PEDOT: PSS on PV parameters of  $\text{KSnI}_3$ -based PSC.



**Fig. 8.** (a) Efficiency vs thickness of the absorber layer. (b) J-V curves with function of absorber layer thickness.

absorbed photons, leading to higher EQE,  $J_{SC}$ , and overall improved performance [47]. This enhancement is also evident in the J-V curves (Fig. 8b). As the absorber layer thickness exceeds 550 nm, both  $V_{OC}$  and FF parameters decrease. Optimum thickness value for  $\text{KSnl}_3$ -based PSC is 550 nm. The maximum efficiency goes up to 23.08 % together with  $V_{OC}$  is 1.57 V,  $J_{SC}$  is 16.90  $\text{mA}/\text{cm}^2$  and FF is 86.59 % at a thickness of 550 nm.

### 3.3.2. Impact of $N_t$

Similarly, with the HTL influence, there is a lack of substantial change in the PV parameters until an  $N_t$  value of  $10^{13} \text{ cm}^{-3}$  is reached. These PV parameters exhibit a decline when a high defect concentration is present. A heightened defect concentration within a low-quality perovskite layer results in an increased number of non-radiative recombination centers, consequently deteriorating PV parameters of PSC. This degradation can be attributed to alterations in the diffusion length of charge carriers and their lifetime. While a low  $N_t$  value might contribute to high PCE in simulated PSCs, the elevated fabrication cost is a deterrent. Moreover, a low  $N_t$  value does not accurately reflect real-world conditions due to the instability of such perovskites under humid conditions, leading to partial degradation. Therefore, we propose  $N_t$  values ranging from  $10^{13}$  to  $10^{15} \text{ cm}^{-3}$  for the building of high-performance PSCs with reasonable stability. The optimized  $N_t$  is  $1 \times 10^{13} \text{ cm}^{-3}$  for  $\text{KSnl}_3$  perovskite layer at which it has achieved the

maximum PCE of 23.08 %, as demonstrated in Fig. 9a. The J-V plot of  $\text{KSnl}_3$  PSCs based on the  $N_t$  of the absorber layer is simulated and demonstrated in Fig. 9b. For perovskite layers when  $N_t$  is increased, the undesirable recombination rate also rises, attributed to the formation of defects that act as dangling bonds, serving as trap state for the charge carriers. This enhancement in recombination leads to fall in  $J_{SC}$ , which is subsequently responsible for the decrement in FF of solar devices. The device PCE also decreased from 23.08 % to 7.85 %, when  $N_t$  was increased from  $10^{13}$  to  $10^{20} \text{ cm}^{-3}$ . Such an increasing amount of recombination resulted in a sharp fall in PCE of PSC.

### 3.4. Optimized device

The optimized ETL and HTL are  $\text{WS}_2$  and PEDOT: PSS respectively with the Au (gold) as metal back contact. The optimized parameters such as 1) Thickness: PEDOT: PSS (250 nm),  $\text{KSnl}_3$  (550 nm),  $\text{WS}_2$  (100 nm) and FTO (400 nm); 2)  $N_A$ : PEDOT: PSS ( $10^{20} \text{ cm}^{-3}$ ) and 3)  $N_t$ : PEDOT: PSS ( $1 \times 10^{14} \text{ cm}^{-3}$ ),  $\text{KSnl}_3$  ( $1 \times 10^{13} \text{ cm}^{-3}$ ) and  $\text{WS}_2$  ( $1 \times 10^{13} \text{ cm}^{-3}$ ). The PSC structure and energy band diagram of the optimized device demonstrated in Fig. 10. The optimized PCE of 23.08 % with  $V_{OC} = 1.57 \text{ V}$ ,  $J_{SC} = 16.90 \text{ mA}/\text{cm}^2$ , and FF of 86.59 % has been obtained. The JV and QE curves of optimized PSC are illustrated in Fig. 11(a-b).

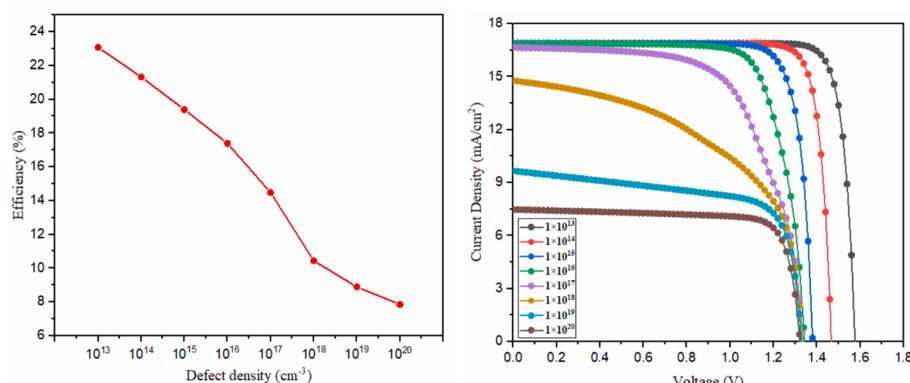


**Fig. 9.** (a) Efficiency vs  $N_t$  of the absorber layer and (b) Effects of  $N_t$  on the J-V characteristics of  $\text{KSnl}_3$ -based PSCs.

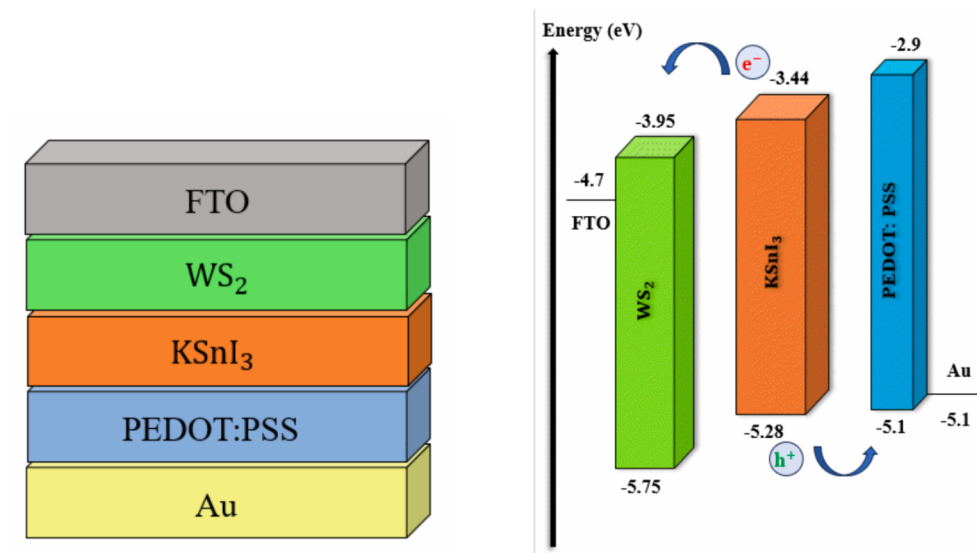


Fig. 10. Architecture and band alignment diagram of optimized PSC.

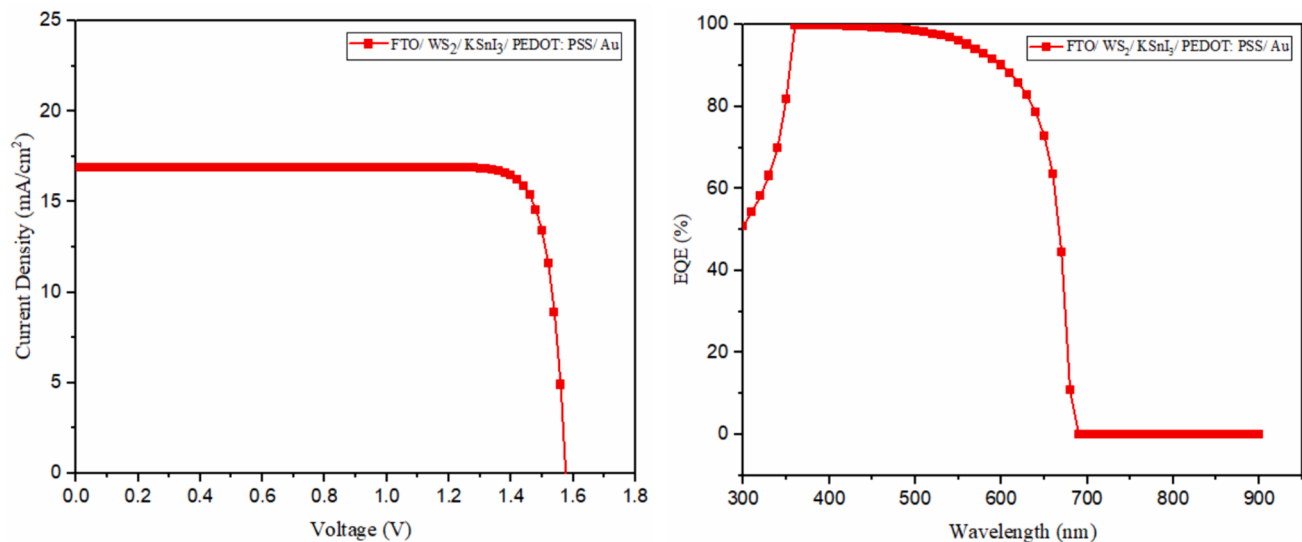


Fig. 11. (a) J-V and (b) QE plot of optimized device.

### 3.5. Machine learning

In this work, python is employed for the prediction of factors affecting the performance of the PSC. Due to its robustness to overfitting and optimal complexity, the Random Forest algorithm was used for the training and testing [48]. The researchers noted that more powerful rivals, like neural networks and deep neural networks, acquire needless complexity, leading to overfitting and reduced performance [49,50]. Considering the relatively small size of the dataset and its high complexity, compiling a larger set of records would be beneficial. The research focused on reducing the dataset's complexity to improve the model's accuracy. By employing Scikit-Learn, influence of every feature on the entire predictive performance of the ML model was observed. The eleven most important features were identified, and their relative importance was shown in Fig. 12. It has shown that the features such as thickness,  $N_t$ ,  $N_A$ , of the HTL were found to be the most responsible in differentiating between the performance of two distinct PSCs. The outcomes guide for the design of new solar cells. Subsequently, a new model was built using the selected important features aiming to achieve a similar level of performance while reducing the model's size due to the

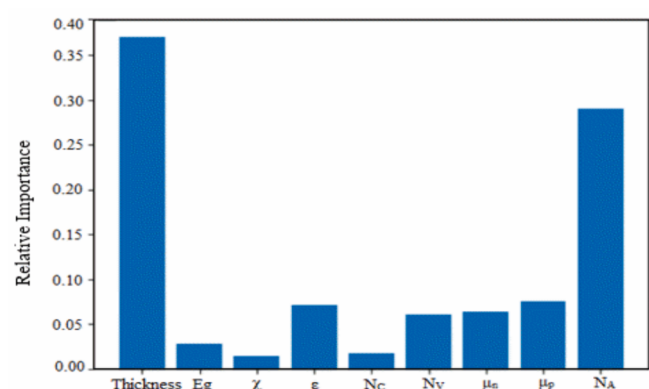


Fig. 12. Different features with relative importance in the ML model.

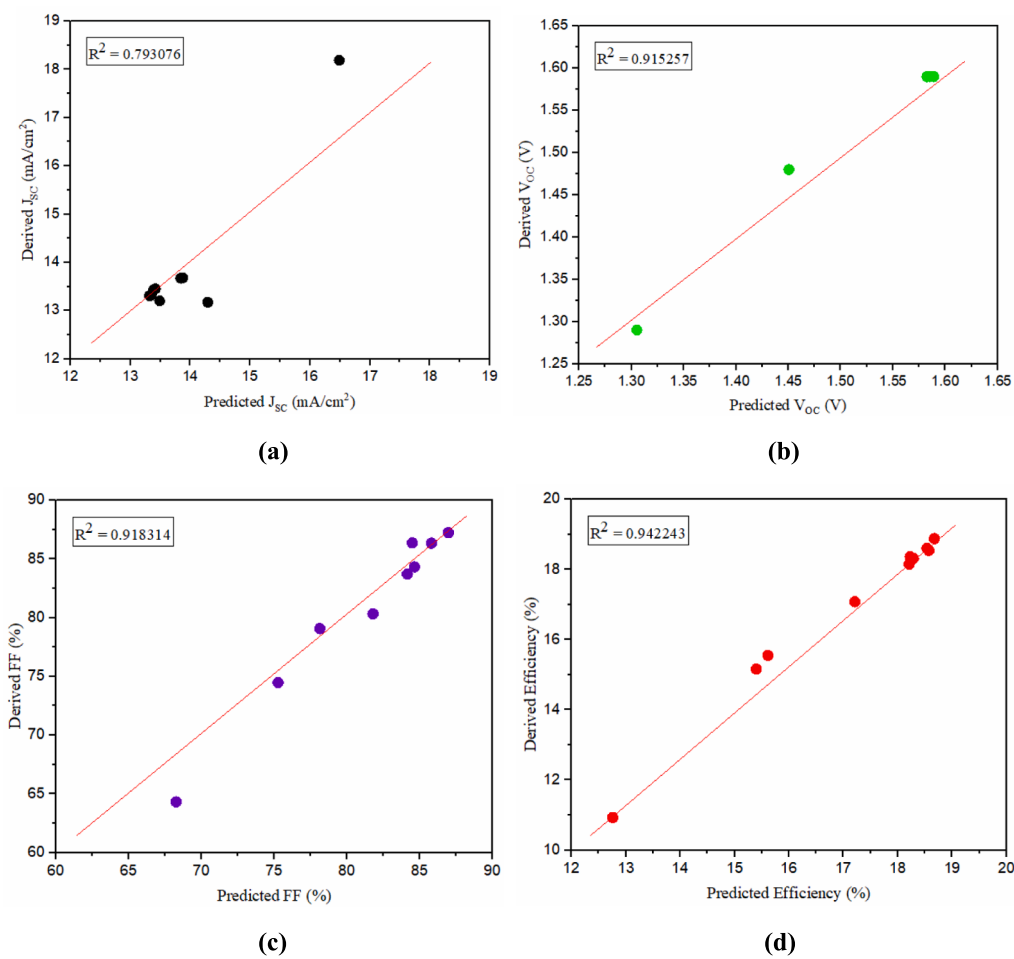


Fig. 13. Derived and predicted values of PV parameters.

fewer features used. The model results were measured and illustrated in Fig. 13 (a-d). Ideally, the slope of plots is near to 1, indicating accurate predictions. The ML model achieved a mean accuracy of 0.89 % and mean  $R^2$  of 0.8921 between actual and predicted values for each target feature. While the accuracy might not be extremely high, the results are encouraging for further investigation and bridging the gap between artificial intelligence and materials science. The model trained for large input data which leads to highly efficient and realistic results.

#### 4. Conclusions

This work comprises analysis of KSnI<sub>3</sub>-based PSC with the various HTLs. The effect of distinct parameters, including thickness of perovskite absorber layer and HTL, as well as N<sub>A</sub> and N<sub>t</sub> have been examined using SCAPS-1D. The ML model was used to predict the performance of the PSCs. The study demonstrated PEDOT: PSS as a promising HTL that could replace the expensive and less-conductive Spiro-OMeTAD. The maximum PCE of 23.08 % was obtained for the configuration of FTO/WS<sub>2</sub>/KSnI<sub>3</sub>/PEDOT: PSS/Au. The SCAPS-1D outcomes, deduced that the optimized thickness of HTL was 200 nm, with N<sub>t</sub> of  $1 \times 10^{14} \text{ cm}^{-3}$  and a N<sub>A</sub> of  $1 \times 10^{20} \text{ cm}^{-3}$  results in maximum PCE. The optimized thickness of the KSnI<sub>3</sub> layer is 550 nm and at N<sub>t</sub> of  $1 \times 10^{13} \text{ cm}^{-3}$  for an efficient PSC. The incorporation of the ML approach provided enhanced insight into the critical factors involved in designing and fabricating solar cells. The ML model demonstrated an accuracy score of 89 % in predicting the performance metrics of PSCs. The device PCE improved beyond 23 % by optimizing parameters such as thickness of absorber layer and HTL, N<sub>t</sub> and N<sub>A</sub>. The study focused on proper optimization of perovskite

absorber layer and HTL for advanced and efficient architecture of KSnI<sub>3</sub>-based PSC. A precise and powerful model can be trained by providing a large number of inputs to ML. With the series of this study, we can study the lead free and other potential material to optimize the performance of PSCs using the ML model.

#### CRediT authorship contribution statement

**Rahul Kundara:** Conceptualization, Data curation, Investigation, Methodology, Software, Validation, Writing – original draft. **Sarita Baghel:** Formal analysis, Project administration, Supervision, Writing – review & editing.

#### Declaration of competing interest

The authors declare that they have no known competing financial interests or personal relationships that could have appeared to influence the work reported in this paper.

#### Data availability

Data will be made available on request.

#### Acknowledgment

The author, Rahul Kundara is thankful to Delhi Technological University, New Delhi for providing a junior research fellowship. We are very grateful to Marc Burgelman, the Electronics and Information

Systems (ELIS), University of Gent, Belgium, for providing us with SCAPS-1D software.

## References

- [1] A. Singha, A. Paul, S. Koul, V. Sharma, S. Mallick, K.R. Balasubramaniam, D. Kabra, Stable and efficient large area 4T Si/perovskite tandem photovoltaics with sputtered transparent contact, *Solar RRL* 7 (2023) 2300117, <https://doi.org/10.1002/solr.202300117>.
- [2] N. Rai, S. Rai, P.K. Singh, P. Lohia, D.K. Dwivedi, Analysis of various ETL materials for an efficient perovskite solar cell by numerical simulation, *J. Mater. Sci. Mater. Electron.* 31 (2020) 16269–16280, <https://doi.org/10.1007/s10854-020-04175-z>.
- [3] I. Elango, M. Selvamani, P.C. Ramamurthy, AV. Kesavan, Studying VOC in lead free inorganic perovskite photovoltaics by tuning energy bandgap and defect density, *Ceram. Int.* 48 (2022) 29414–29420. <https://doi.org/10.1016/j.ceramint.2022.06.125>.
- [4] M.S. Islam, K. Sobayel, A. Al-Kahtani, M.A. Islam, G. Muhammad, N. Amin, M. Shahiduzzaman, M. Akhtaruzzaman, Defect study and modelling of SnX3-based perovskite solar cells with SCAPS-1D, *Nanomaterials* 11 (2021), <https://doi.org/10.3390/nano11051218>.
- [5] N. Lakhdar, A. Hima, Electron transport material effect on performance of perovskite solar cells based on CH3NH3GeI3, *Opt Mater (AMST)* 99 (2020), <https://doi.org/10.1016/j.optmat.2019.109517>.
- [6] S. Mushtaq, S. Tahir, A. Ashfaq, R. Sebastian Bonilla, M. Haneef, R. Saeed, W. Ahmad, N. Amin, Performance optimization of lead-free MASnBr 3 based perovskite solar cells by SCAPS-1D device simulation, *Sol. Energy* 249 (2023) 401–413, <https://doi.org/10.1016/j.solener.2022.11.050>.
- [7] N.K. Noel, S.D. Stranks, A. Abate, C. Wehrfennig, S. Guarnera, A.A. Haghhighirad, A. Sadhanala, G.E. Eperon, S.K. Pathak, M.B. Johnston, A. Petrozza, L.M. Herz, H. J. Snaith, Lead-free organic-inorganic tin halide perovskites for photovoltaic applications, *Energy Environ. Sci.* 7 (2014) 3061–3068, <https://doi.org/10.1039/c4ee01076k>.
- [8] M.G. Ju, M. Chen, Y. Zhou, H.F. Garces, J. Dai, L. Ma, N.P. Padture, X.C. Zeng, Earth-abundant nontoxic titanium(IV)-based vacancy-ordered double perovskite halides with Tunable 1.0 to 1.8 eV bandgaps for photovoltaic applications, *ACS Energy Lett.* 3 (2018) 297–304, <https://doi.org/10.1021/acsenergylett.7b01167>.
- [9] Z. Zhang, X. Li, X. Xia, Z. Wang, Z. Huang, B. Lei, Y. Gao, High-quality (CH3NH3) 3Bi219 film-based solar cells: pushing efficiency up to 1.64%, *J. Phys. Chem. Lett.* 8 (2017) 4300–4307, <https://doi.org/10.1021/acs.jpclett.7b01952>.
- [10] M. Wang, P. Zeng, S. Bai, J. Gu, F. Li, Z. Yang, M. Liu, High-quality sequential-vapor-deposited Cs2AgBiBr 6 thin films for lead-free perovskite solar cells, *Solar RRL* 2 (2018), <https://doi.org/10.1002/solr.201800217>.
- [11] Y. Zong, Y. Zhou, Y. Zhang, Z. Li, L. Zhang, M.G. Ju, M. Chen, S. Pang, X.C. Zeng, N. P. Padture, Continuous grain-boundary functionalization for high-efficiency perovskite solar cells with exceptional stability, *Chem* 4 (2018) 1404–1415, <https://doi.org/10.1016/j.chempr.2018.03.005>.
- [12] G. Pindolia, S.M. Shinde, P.K. Jha, Non-leaded, KSnI3 based perovskite solar cell: A DFT study along with SCAPS simulation, *Mater. Chem. Phys.* 297 (2023), <https://doi.org/10.1016/j.matchemphys.2023.127426>.
- [13] A. Tara, V. Bharti, S. Sharma, R. Gupta, Device simulation of FASnI3 based perovskite solar cell with Zn(O0.3, 50.7) as electron transport layer using SCAPS-1D, *Opt Mater (amst)* 119 (2021), <https://doi.org/10.1016/j.optmat.2021.111362>.
- [14] W. Yan, Y. Liu, Y. Zang, J. Cheng, Y. Wang, L. Chu, X. Tan, L. Liu, P. Zhou, W. Li, Z. Zhong, Machine learning enabled development of unexplored perovskite solar cells with high efficiency, *Nano Energy* 99 (2022) 107394, <https://doi.org/10.1016/j.nanoen.2022.107394>.
- [15] S. Rai, B.K. Pandey, D.K. Dwivedi, Modeling of highly efficient and low cost CH3NH3Pb(I-xClx)3 based perovskite solar cell by numerical simulation, *Opt Mater (amst)*, 100 (2020), <https://doi.org/10.1016/j.optmat.2019.109631>.
- [16] M. Kumar, A. Raj, A. Kumar, A. Anshul, An optimized lead-free formamidinium Sn-based perovskite solar cell design for high power conversion efficiency by SCAPS simulation, *Opt Mater (amst)*, 108 (2020), <https://doi.org/10.1016/j.optmat.2020.110213>.
- [17] M.K. Hossain, G.F.I. Toki, A. Kuddus, M.H.K. Rubel, M.M. Hossain, H. Bencherif, M.F. Rahman, M.R. Islam, M. Mushtaq, An extensive study on multiple ETL and HTL layers to design and simulation of high-performance lead-free CsSnCl3-based perovskite solar cells, *Sci. Rep.* 13 (2023), <https://doi.org/10.1038/s41598-023-28506-2>.
- [18] A.A. Kanoun, M.B. Kanoun, A.E. Merad, S. Goumri-Said, Toward development of high-performance perovskite solar cells based on CH3NH3GeI3 using computational approach, *Sol. Energy* 182 (2019) 237–244, <https://doi.org/10.1016/j.solener.2019.02.041>.
- [19] S. Bhattacharai, T.D. Das, Optimization of carrier transport materials for the performance enhancement of the MAGel3 based perovskite solar cell, *Sol. Energy* 217 (2021) 200–207, <https://doi.org/10.1016/j.solener.2021.02.002>.
- [20] S.Z. Haider, H. Anwar, M. Wang, Theoretical device engineering for high-performance perovskite solar cells using CuSCN as hole transport material boost the efficiency above 25%, *Physica Status Solidi (A) Applications and Materials Science* 216 (2019) <https://doi.org/10.1002/pssa.201900102>.
- [21] B. Li, H. Di, B. Chang, R. Yin, L. Fu, Y.N. Zhang, L. Yin, Efficient passivation strategy on Sn related defects for high performance all-inorganic CsSnI3 perovskite solar cells, *Adv. Funct. Mater.* 31 (2021), <https://doi.org/10.1002/adfm.202007447>.
- [22] U. Mandadapu, S.V. Vedanayakam, K. Thyagarajan, Simulation and analysis of lead based perovskite solar cell using SCAPS-1D, *Indian. J. Sci. Technol.* 10 (2017) 1–8, <https://doi.org/10.17485/ijst/2017/v10i11/110721>.
- [23] K. Deepthi Jayan, V. Sebastian, Comprehensive device modelling and performance analysis of MASnI3 based perovskite solar cells with diverse ETM, HTM and back metal contacts, *Sol. Energy* 217 (2021) 40–48, <https://doi.org/10.1016/j.solener.2021.01.058>.
- [24] O. Ahmad, A. Rashid, M.W. Ahmed, M.F. Nasir, I. Qasim, Performance evaluation of Au/p-CdTe/Cs2TiI6/n-TiO2/ITO solar cell using SCAPS-1D, *Opt Mater (amst)*, 117 (2021), <https://doi.org/10.1016/j.optmat.2021.111105>.
- [25] Y. Gan, X. Bi, Y. Liu, B. Qin, Q. Li, Q. Jiang, P. Mo, Numerical investigation energy conversion performance of tin-based perovskite solar cells using cell capacitance simulator, *Energies (basel)*, 13 (2020), <https://doi.org/10.3390/en13225907>.
- [26] M.K. Hossain, A.A. Arnab, R.C. Das, K.M. Hossain, M.H.K. Rubel, M.F. Rahman, H. Bencherif, M.E. Emetere, M.K.A. Mohammed, R. Pandey, Combined DFT, SCAPS-1D, and wxAMPS frameworks for design optimization of efficient Cs2BiAgI6-based perovskite solar cells with different charge transport layers, *RSC Adv.* 12 (2022) 34850–34873, <https://doi.org/10.1039/d2ra06734j>.
- [27] S.P. Ong, W.D. Richards, A. Jain, G. Hautier, M. Kocher, S. Cholia, D. Gunter, V. L. Chevrier, K.A. Persson, G. Ceder, Python Materials genomics ( pymatgen): a robust, open-source python library for materials analysis, *Comput. Mater. Sci.* 68 (2013) 314–319, <https://doi.org/10.1016/j.commatsci.2012.10.028>.
- [28] L. Ward, A. Dunn, A. Faghaninia, N.E.R. Zimmermann, S. Bajaj, Q. Wang, J. Montoya, J. Chen, K. Bystrom, M. Dylla, K. Chard, M. Asta, K.A. Persson, G. J. Snyder, I. Foster, A. Jain, Matminer: An open source toolkit for materials data mining, *Comput. Mater. Sci.* 152 (2018) 60–69, <https://doi.org/10.1016/j.commatsci.2018.05.018>.
- [29] R.T. Yarlagadda, Novateur publications international journal of innovations in engineering research and technology [IJIERT] python engineering automation to advance artificial intelligence and machine learning systems, 5 (2018). <https://ssrn.com/abstract=3797347>.
- [30] Z. Jin, J. Shang, Q. Zhu, C. Ling, W. Xie, B. Qiang, RFRSF: Employee turnover prediction based on random forests and survival analysis. In: Web Information Systems Engineering–WISE 2020: 21st International Conference, Amsterdam, The Netherlands, October 20–24, 2020, Proceedings, Part II 21 2020 (pp. 503–515). Springer International Publishing.
- [31] K. Sobayel, M. Akhtaruzzaman, K.S. Rahman, M.T. Ferdaous, Z.A. Al-Mutairi, H. F. Alharbi, N.H. Alharthi, M.R. Karim, S. Hasmady, N. Amin, A comprehensive defect study of tungsten disulfide (WS2) as electron transport layer in perovskite solar cells by numerical simulation, *Results Phys.* 12 (2019) 1097–1103, <https://doi.org/10.1016/j.rinp.2018.12.049>.
- [32] G. Pindolia, S.M. Shinde, Effect of organic charge transport layers on unleaded KSnI3 based perovskite solar cell, *Results in Optics*, 12 (2023) 100469, <https://doi.org/10.1016/j.rio.2023.100469>.
- [33] Y. Xia, S. Dai, Review on applications of PEDOTs and PEDOT:PSS in perovskite solar cells, *J. Mater. Sci. Mater. Electron.* 32 (2021) 12746–12757, <https://doi.org/10.1007/s10854-020-03473-w>.
- [34] L. Zhao, J. Mou, L. Zhu, J. Song, Synergistic effect of NiO and Spiro-OMeTAD for hole transfer in perovskite solar cells, *J. Electron. Mater.* 50 (2021) 6512–6517, <https://doi.org/10.1007/s11664-021-09193-z>.
- [35] Q. Du, Z. Shen, C. Chen, F. Li, M. Jin, H. Li, C. Dong, J. Zheng, M. Ji, M. Wang, Spiro-OMeTAD:Sb2S3 hole transport layer with triple functions of overcoming lithium salt aggregation, long-term high conductivity, and defect passivation for perovskite solar cells, *Solar RRL*, 5 (2021), <https://doi.org/10.1002/solr.202100622>.
- [36] C. Zuo, L. Ding, Modified PEDOT layer makes a 1.52 V Voc for perovskite/PCBM solar cells, *Adv. Energy Mater.* 7 (2017), <https://doi.org/10.1002/aenm.201601193>.
- [37] D. Liu, Y. Li, Y. Yuan, Q. Hong, G. Shi, D. Yuan, J. Wei, C. Huang, J. Tang, M. K. Fung, Improved performance of inverted planar perovskite solar cells with F4-TCNQ doped PEDOT: PSS hole transport layers, *J. Mater. Chem. A* 5 (2017), <https://doi.org/10.1039/C6TA10212C>.
- [38] S. Li, Y.L. Cao, W.H. Li, Z.S. Bo, A brief review of hole transporting materials commonly used in perovskite solar cells, *Rare Met.* 40 (2021) 2712–2729, <https://doi.org/10.1007/s12598-020-01691-z>.
- [39] H. Sharma, V.K. Verma, R.C. Singh, P.K. Singh, A. Basak, Numerical analysis of high-efficiency CH3NH3PbI3 perovskite solar cell with PEDOT: PSS hole transport material using SCAPS 1D simulator, *J. Electron. Mater.* 52 (2023) 4338–4350, <https://doi.org/10.1007/s11664-023-10257-5>.
- [40] M.A. Naliniya, C. Awino, H. Barasa, V. Odari, F. Gaitho, B. Omogo, M. Mageto, Numerical study of lead free CsSn0.5Ge0.5I3 perovskite solar cell by SCAPS-1D, *Optik* 248 (2021) 168060, <https://doi.org/10.1016/j.jilgeo.2021.168060>.
- [41] N. Marinova, W. Tress, R. Humphry-Baker, M.I. Dar, V. Bojinov, S.M. Zakeeruddin, M.K. Nazeeeruddin, M. Grätzel, Light harvesting and charge recombination in CH3NH3PbI3 perovskite solar cells studied by hole transport layer thickness variation, *ACS Nano* 9 (2015) 4200–4209, <https://doi.org/10.1021/acsnano.5b00447>.
- [42] F. Azri, A. Meftah, N. Sengouga, A. Meftah, Electron and hole transport layers optimization by numerical simulation of a perovskite solar cell, *Sol. Energy* 181 (2019) 372–378, <https://doi.org/10.1016/j.solener.2019.02.017>.
- [43] B.L. Williams, V. Zardetto, B. Kniknie, M.A. Verheijen, W.M.M. Kessels, M. Creatore, The competing roles of i-ZnO in Cu(In, Ga)Se2 solar cells, *Sol. Energy Mater. Sol. Cells* 157 (2016) 798–807, <https://doi.org/10.1016/j.solmat.2016.07.049>.
- [44] F. Paquin, J. Rivnay, A. Salleo, N. Stingelin, C. Silva-Acuña, Multi-phase microstructures drive exciton dissociation in neat semicrystalline polymeric

- semiconductors, J Mater Chem C Mater. 3 (2015) 10715–10722, <https://doi.org/10.1039/c5tc02043c>.
- [45] S.J. Yoo, J.H. Lee, J.H. Lee, J.J. Kim, Doping-concentration-dependent hole mobility in a ReO<sub>3</sub> doped organic semiconductor of 4,4',4''-tris(N-(2-naphthyl)-N-phenyl-amino)-tri phenylamine, Appl. Phys. Lett. 102 (2013), <https://doi.org/10.1063/1.4804141>.
- [46] F. Anwar, R. Mahbub, S.S. Satter, S.M. Ullah, Effect of different HTM layers and electrical parameters on ZnO nanorod-based lead-free perovskite solar cell for high-efficiency performance, Int. J. Photoenergy 2017 (2017), <https://doi.org/10.1155/2017/9846310>.
- [47] L. Hao, T. Li, X. Ma, J. Wu, L. Qiao, X. Wu, G. Hou, H. Pei, X. Wang, X. Zhang, A tin-based perovskite solar cell with an inverted hole-free transport layer to achieve high energy conversion efficiency by SCAPS device simulation, Opt. Quant. Electron. 53 (2021), <https://doi.org/10.1007/s11082-021-03175-5>.
- [48] W. McKinney, Data structures for statistical computing in python, InProceedings of the 9th Python in Science Conference 2010 Jun 28 (Vol. 445, No. 1, pp. 51-56). DOI: 10.25080/Majora-92bf1922-00a.
- [49] J. Schmidhuber, Deep learning in neural networks: an overview, Neural Netw. 61 (2015) 85–117, <https://doi.org/10.1016/j.neunet.2014.09.003>.
- [50] M. Hasanzadeh Azar, S. Aynehband, H. Abdollahi, H. Alimohammadi, N. Rajabi, S. Angizi, V. Kamraninejad, R. Teimouri, R. Mohammadpour, A. Simchi, SCAPS Empowered Machine Learning Modelling of Perovskite Solar Cells: Predictive Design of Active Layer and Hole Transport Materials, Photonics. 10 (2023). DOI: 10.3390/photonics10030271.